Food Chemistry 422 (2023) 136162

Contents lists available at ScienceDirect

Food Chemistry

journal homepage: www.elsevier.com/locate/foodchem

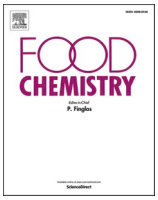

Effects of liquid nitrogen freezing at different temperatures on the quality and flavor of Pacific oyster (*Crassostrea gigas*)

Xiaoyu Teng [a], Yu Liu [a], Lipin Chen [a,*], Changhu Xue [a], Zhaojie Li [a,b,*]

[a] College of Food Science and Engineering, Ocean University of China, No.5, Yu-Shan Road, Qingdao, Shandong Province, PR China
[b] Collaborative Innovation Center of Seafood Deep Processing, Dalian Polytechnic University, Dalian 116034, PR China

ARTICLE INFO

Keywords:
Liquid nitrogen freezing
Quality
Flavor
Pacific oyster (*Crassostrea gigas*)

ABSTRACT

This study aimed to evaluate the effects of different liquid nitrogen freezing (LNF) temperatures (-20, −40, −60, −80, and −100 °C) on the water holding capacity, texture, microstructure, and flavor of *Crassostrea gigas* (*C. gigas*). The results showed that −40 °C LNF, −60 °C LNF, and −80 °C LNF improved the water holding capacity of *C. gigas* ($P < 0.05$); −60 °C LNF and −80 °C LNF could effectively maintain the hardness of the body trunk and adductor muscles. Compared with −20 °C refrigerator freezing (RF), the LNF group could form smaller ice crystals and thus reduce the damage to the muscle cell structure damage, especially LNF at −80 °C. Gas chromatography-ion mobility spectrometry (GC-IMS) and e-nose results indicated that −80 °C LNF maintained the flavor profile of few aldehydes and alcohols compared to other freezing groups. Therefore, −80 °C LNF effectively improved the quality and maintain the flavor characteristics of frozen *C. gigas*.

1. Introduction

Oyster is currently the most economical shellfish produced, and distributed in coastal areas all over the world (Teng et al., 2022). Among them, the Pacific oyster (*Crassostrea gigas*) is one of the most important species, which is popular among consumers because of its delicious meat, high nutritional value, rich in lipids, and protein (Botta et al., 2020; Peng et al., 2021). However, the rich nutrients, high moisture, and endogenous proteases of oysters are highly susceptible to quality deterioration under the action of enzymes and microorganisms, resulting in changes in flavor, texture, and color (Sun et al., 2019).

Freezing is an effective method to extend the shelf life of aquatic products, which can effectively inhibit the growth and reproduction of microorganisms, reduce the activity of enzymes, and slow down the oxidation of lipids and proteins (Espinoza Rodezno et al., 2013; Sun et al., 2019). However, the size, shape, and location of ice crystal formed determine the nutrient loss, texture, flavor, and color changes of frozen foods (Zhu, Zhou, & Sun, 2019). Traditional freezing methods have slow freezing rates, such as air freezing and submersion freezing (Gao, Hou, & Zeng, 2019). Slow-rate freezing usually forms large ice crystals in the extracellular region of the food, which may lead to undesirable quality changes, disrupting the microstructure of the food and causing deterioration in texture, color, and water retention of the food (Li, Zhu, & Sun, 2018).

Liquid nitrogen freezing is a fast freezing method that rapidly freezes foods by instantaneous vaporization of liquid nitrogen and speeds up the heat transfer process (Lopkulkiaert, Prapatsornwattana, & Rungsardthong, 2009). Compared with traditional freezing technology, liquid nitrogen freezing has the advantages of a high heat transfer coefficient, fast freezing speed, and small ice crystal formation (Yang et al., 2021). However, improper liquid nitrogen freezing also has some disadvantages, such as the freezing temperature being too low, which the phenomenon of food freezing cracks will occur, resulting in the quality of food quality decline (Al-Dalali, Li, & Xu, 2021). Therefore, it is important to study the different temperatures of liquid nitrogen freezing. The current research on liquid nitrogen freezing is mainly focused on fish, shrimp, crabs, fruits, and plants (Yang et al., 2022). As reported by Yang et al. (2022), controlling the temperature of liquid nitrogen during the freezing process effectively improves the quality of aquatic products, and −95 °C LNF could reduce the thawing loss, cooking loss, lightness values of fish. However, there are relatively few studies on liquid nitrogen frozen oysters, especially concerning flavor changes. Gas chromatography-ion mobility spectrometry (GC-IMS) is a new detection technology that is widely used and has the advantages of fast detection speed and simple operation (Chen et al., 2022).

The main objective of this study is to investigate the effect of liquid

* Corresponding authors.
E-mail addresses: cchenlp@163.com (L. Chen), lizhaojie@ouc.edu.cn (Z. Li).

https://doi.org/10.1016/j.foodchem.2023.136162
Received 1 February 2023; Received in revised form 2 April 2023; Accepted 11 April 2023
Available online 18 April 2023

nitrogen freezing at different temperatures (−20, −40, −60, −80 and −100 °C) on the quality and flavor of oysters. The effect on oysters quality are investigated by measuring the freezing rate, water holding capacity, hardness, and microstructure at different liquid nitrogen temperatures. Furthermore, the changes of flavor components are further analyzed by GC-IMS and electronic nose to provide a theoretical basis for further improving the product quality of the oyster production industry.

2. Materials and methods

2.1. Experimental design

C. gigas was purchased from a farm (Qingdao, China), and transported quickly to the laboratory in a foam-padded box with ice bags. *C. gigas* were washed and shucked, and then divided into seven groups randomly, including Fresh samples; −20 °C refrigerator freezing (RF) as the control group; −20, −40, −60, −80, and −100 °C LNF. Set the running temperature of the liquid nitrogen quick-freezer refrigerator to −20, −40, −60, −80, and −100 °C respectively. The samples were put into the quick-freezer under the required temperature, and when the center temperature of the sample reached −18 °C, the freezing was considered to be completed. All samples were stored in a −20 °C refrigerator before analysis. For thawing, they were uniformly placed in a 4 °C refrigerator and considered to be thawed when the central temperature reached 4 °C (Yang et al., 2021).

2.2. Freezing curves and freezing rates

The temperature of the sample during freezing was measured with a temperature sensor (the refrigerator comes with a thermocouple). A temperature sensor probe was inserted into the center of the *C. gigas* and the temperature and time date were recorded every two seconds, terminating the freeze when the central temperature dropped to −18 °C. Freezing curves were plotted according to *C. gigas* center temperature change over time. The freezing rate was calculated by referring to the method of Yang et al. (2020) with the following equation:

$$Freezing\ curves(^{\circ}C/min) = \frac{T_2 - T_1}{t_2 - t_1} \times 60$$

In the formula: $T_2 = -1^{\circ}C$, $T_1 = -5^{\circ}C$, t_2-t_1 represents the time taken to drop from −1°C to −5°C.

2.3. Water holding capacity (WHC)

2.3.1. Centrifugal loss

Centrifugal loss was determined following the method previously described by Li et al. (2022). Briefly, the surface water of the thawed sample was removed and the sample was weighed (m_1). The sample was wrapped in filter paper placed in a centrifuge tube with cotton at the bottom and centrifuged at 3000×g for 10 min. After centrifugation, the filter paper was removed and the sample was weighed (m_2) again. Centrifugal loss was calculated using the following formula:

$$Centrifugalloss(\%) = \frac{m_1 - m_2}{m_1} \times 100\%$$

2.3.2. Steaming loss

Steaming loss was determined according to the method of Yang et al. (2022), with a slight modification. The thawed samples were dried and weighed (M_1) and then heated at 100 °C for 10 min. After cooling to room temperature, the water on the surface of the sample was blotted with filter paper and the samples were weighed (M_2) again. The steaming loss was obtained as follows:

$$Steamingloss(\%) = \frac{M_1 - M_2}{M_1} \times 100\%$$

2.3.3. Thawing loss

Thawing loss was carried out according to the slightly modified method of Sun et al. (2019). In brief, the sample mass before thawing was weighed (W_1) and thawed at 4 °C refrigerator until the central temperature of the sample reached 4 °C. The sample was then dried on filter paper and the sample mass weighed (W_2) again. Thawing loss was calculated using the following equation:

$$Thawingloss(\%) = \frac{W_1 - W_2}{W_1} \times 100\%$$

2.4. Hardness

Hardness was determined using a slightly modified method by Ma, Mei, and Xie (2021). The body trunk and adductor muscles of thawed *C. gigas* were separated and the hardness of the body trunk and adductor muscles was determined using the TPA mode of a mass spectrometer (TMS-TOUCH, Food Technology Co., US). The measurement conditions were as follows: the test speed was 60 mm/min, the deformation was 50%, and the trigger force was 0.5 N.

2.5. Light microscopy

The microstructure of *C. gigas* muscle was observed according to the method described in detail previously with some modifications (Jiang et al. (2019). The samples were processed using an indirect method of isothermal freezing alternative technique. The adductor muscles sections of *C. gigas* were seperated and fixed in Carnoy's solution (75% absolute ethanol, 25% acetic acid, v/v) for 24 h. The samples were separately dehydrated in 75%, 85%, 95% ethanol, and anhydrous ethanol then washed in xylene. The samples were fixed in an embedding agent in a slicing machine and then sliced with the slicer into 10 μm thick sections perpendicular to the direction of the *C. gigas* muscle fibre. Afterward, dehydration was carried out in 70%, 80%, 90%, and anhydrous ethanol for 3 min each time. The slices were stained with 10% eosin for 10 min, washed with distilled water for 5 min, dried, and sealed with neutral resin. Finally, the slices were observed with a light microscope equipped with a digital camera.

2.6. Electronic nose

2 g of *C. gigas* was placed in a 20 mL headspace vial. The electronic nose (Airsense Technology Co., Ltd., Germany) was used to analyze *C. gigas*. It consisted of 10 metal oxide sensors with specific identification of different volatile compounds (Chen et al., 2022; Hu et al., 2021), mainly W1C (aromatic compounds), W1W (sulfur compounds, terpenes), W1S (methane, broad range of compounds), W2W (aromatics and organic sulfur compounds), W2S (broad range, alcohols), W3S (methane and aliphatic compounds), W3C (ammonia, aromatic compounds), W5S (nitrous oxides), W5C (alkanes and aromatics) and W6S (hydrocarbons) (Huang et al., 2019). The measurement conditions were as follows: measurement time was 120 s, sample interval was 1 s, and flush time was 60 s.

2.7. Volatile organic compounds (VOCs)

The VOCs of *C. gigas* were assayed with Flavor-spec® gas chromatography-ion mobility spectrometer (GC-IMS) (G.A.S. Technology Co., Ltd., Germany). *C. gigas* (2 g) was placed into a 20 mL headspace injection bottle and incubated at 60 °C (500 rpm, 10 min). The detection method followed the previous research by Wang et al. (2022) with slight modifications. The instrument was equipped with a syringe and an autosampler unit for headspace analysis. 500 μL of sample headspace was automatically injected into the heated syringe (85 °C) of the GC-IMS equipment using a heated syringe (85 °C). VOCs of the *C. gigas* were analyzed using an FS-SE-54-CB capillary column (15 m ×

0.53 mm) at 40 °C. Nitrogen (99.99% purity) was used as the carrier gas: 2 mL/min for 5 min, 100 mL/min for 5 min, and 150 mL/min for 7 min (Chen et al., 2022). LAV (version 2.2.1 – G.A.S., Dortmund, company) was used to process the data. Identification of volatiles was achieved by comparing the mass spectra of the samples with those from the NIST 2014 (National Institute of Standards and Technology, Gaithersburg, USA) and IMS mass spectrometry databases. For the identification of VOCs, retention indices (RI) were calculated using *n*-ketones series (C4-C9) (Jia et al., 2019). All GC-IMS analyses were performed in triplicate.

2.8. Statistical analysis

All experiments were repeated at least three times, and data were expressed as mean ± standard deviation (SD). To analyze the significant differences in these indicators, one-way ANOVA was performed using the Statistical Product and Service Solutions (SPSS) statistical software (version 26.0, IBM, Chicago, USA). $P < 0.05$ was considered as a statistically significant difference.

3. Results and discussion

3.1. Effect of liquid nitrogen freezing at different temperatures on freezing curves and freezing rates of C. gigas

Rapid freezing could significantly improve the quality of frozen meat, the faster the freezing rate, the smaller the ice crystals formed (Ma, Mei, & Xie, 2021). The time–temperature curves of *C. gigas* samples with different freezing treatments were shown in Fig. 1. The freezing rates of the *C. gigas* samples with different freezing treatments were shown in Table 1. The time–temperature profiles could be divided into three phases: (i) precooling stage (or cooling stage): 4 to −1°C; (ii) phase change stage: −1 to −5°C; and (iii) the subcooling stage: −5 to −18 °C (Ma, Mei, & Xie, 2021). The total freezing time of sample was defined as the time required for the temperature to drop from 4 °C to −18 °C. The freezing rate was calculated from the ratio of the temperature and time of the phase change phase. The phase change stage was the time for ice crystal formation and the fast or slow freezing rate directly affected the size, shape, and muscle tissue structure of the ice crystals. In the freezing of oyster samples, treatment with LNF significantly increased the freezing rate. The freezing time of *C. gigas* samples treated with RF was approximately 150 min, which was more than five times longer than that of the −20 °C LNF group, with the −100 °C LNF treatment having the shortest freezing time, 98.12% shorter than that of RF. Similarly, the freezing rate of −20 °C LNF was 7.5 times higher than that of −20 °C RF. The freezing rates of LNF-treated *C. gigas* samples were 0.06 ± 0.06, 0.45 ± 0.03, 1.40 ± 0.03, 2.29 ± 0.12, 3.45 ± 0.15 and 4.45 ± 0.09 °C/min. From the results it could be obtained that as the temperature of liquid nitrogen decreased, the freezing rate increased significantly ($P < 0.05$). As reported by the freezing time of the –115 °C LNF was the shortest, which was 95.41% shorter than that of RF, followed by –95 °C LNF, –75 °C LNF, –55 °C LNF, and –35 °C LNF ($P < 0.05$). The LNF samples could significantly reduce the freezing time, increase the freezing rate and maintain good muscle tissue structure, mainly because the heat transfer coefficient of air was lower than that of liquid nitrogen. During slow freezing, water would first crystallize in the intercellular space, and as the temperature decreased, the water inside the cell kept transferring through the cell membrane to the intercellular space, causing the ice crystals outside the cell to grow and formed irregularly shaped and unevenly distributed, damaging the tissue structure. The process of rapid freezing typically induced a more rapid temperature change, thereby facilitating the crystallization of water both within and outside the cell, resulting in the formation of small ice crystals that exhibited uniform distribution and regular morphology. This process aided in the preservation of the tissue structure of the food product. The results indicated that LNF could effectively reduce the freezing time compared to RF, the freezing rate increases, and the freezing time decreases significantly ($P < 0.05$) as the liquid nitrogen temperature decreases.

Table 1
Freezing rates at different liquid nitrogen temperatures.

Freezing rate	−20 °C RF	−20 °C LNF	−40 °C LNF	−60 °C LNF	−80 °C LNF	−100 °C LNF
(°C/min)	0.06 ± 0.06^{f}	0.45 ± 0.03^{e}	1.40 ± 0.03^{d}	2.29 ± 0.12^{c}	3.45 ± 0.15^{b}	4.45 ± 0.09^{a}

Different letters in each column indicated a significant difference ($P < 0.05$). RF, refrigerator freezing; LNF, liquid nitrogen freezing.

3.2. Effect of liquid nitrogen freezing at different temperatures on WHC of C. gigas

WHC was an important indicator of food quality and was usually evaluated in terms of centrifugal loss, cooking loss, and thawing loss, and the sum of centrifugal loss and thawing loss was juice loss (Wu et al., 2021). Centrifugal loss referred to the ability of meat to retain intrinsic moisture and add moisture, which had implications for both further processing and consumption of the frozen product. As shown in Fig. 2A, centrifugal losses increased significantly ($P < 0.05$) for all the frozen treated compared to the fresh group, with the highest centrifugal losses for the RF-treated *C. gigas* samples, and for the LNF-treated *C. gigas* samples, as the liquid nitrogen temperature decreased, the centrifugal losses for *C. gigas* samples decreased ($P < 0.05$). The centrifugal loss for the −80 °C LNF was 17.54%, a 9.61% reduction in centrifugal loss compared to the RF, which was consistent with the result demonstrated by Wu et al. (2021). Among them, there was no significant difference in centrifugal loss between −40 °C LNF, −60 °C LNF, and −80 °C LNF

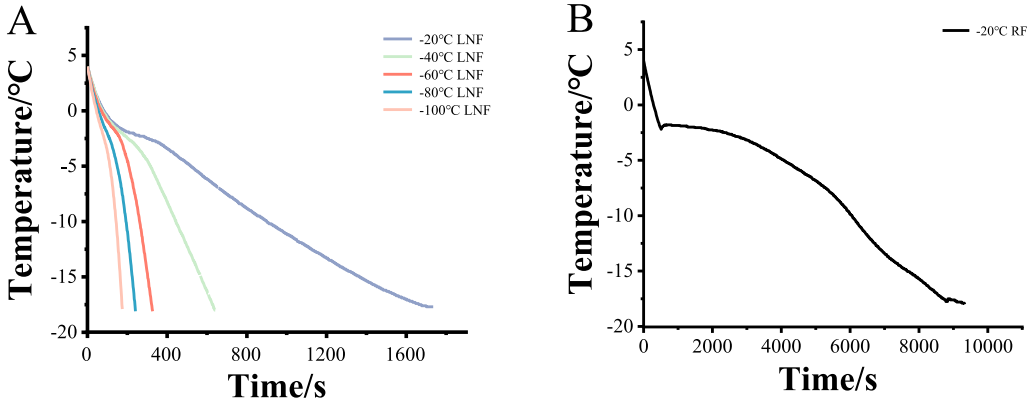

Fig. 1. Freezing curves of *C. gigas* samples with different freezing treatments. (A) Freezing curves of *C. gigas* samples at different LNF temperatures; (B) –20 °C RF.

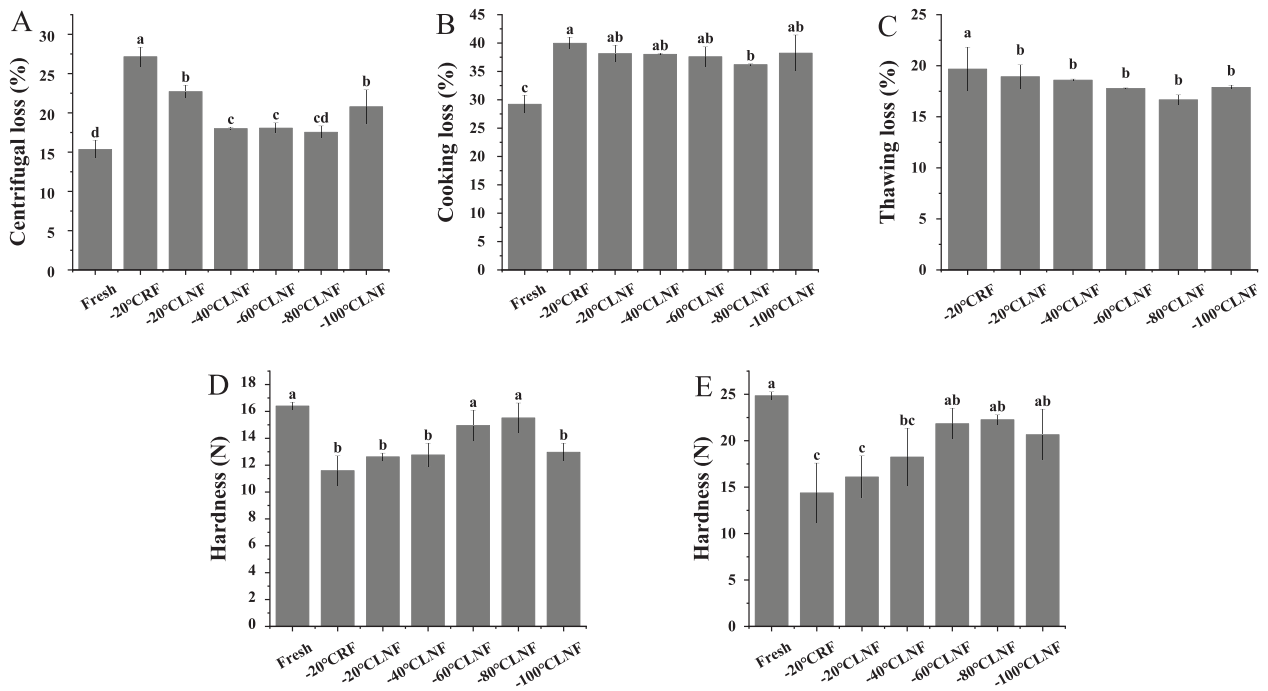

Fig. 2. Changes in (A) centrifugal loss, (B) steaming loss, (C) thawing loss, (D) body trunk hardness, and (E) adductor muscles hardness of *C. gigas* samples with different freezing treatments. Different letters indicate a significant difference ($P < 0.05$).

groups ($P > 0.05$).

Steaming loss generally included the loss of water and soluble substances from the food during steaming (Dalvi-Isfahan, Hamdami, & Le-Bail, 2016). Steaming losses were mainly attributed to structural damage to muscle caused by heat-induced deformation of brothel fibrin (Hong et al., 2013). The trend of steaming losses was similar to that of thawing losses and centrifugal losses. As shown in Fig. 2B, there was a significant difference in steaming loss between RF-treated samples and LNF-treated samples ($P < 0.05$). Then, there was no significant difference between the LNF-treated samples ($P > 0.05$). Except for the Fresh samples, the lowest steaming loss (36.20%) was observed for *C. gigas* samples treated with −80 °C LNF, and the highest steaming loss (39.98%) was observed for *C. gigas* samples treated with −20 °C RF. As the temperature of liquid nitrogen decreased, the steaming loss of *C. gigas* samples decreased and then increased. This result was mainly due to the fact that *C. gigas* samples snap-frozen in liquid nitrogen could produce small and regular ice crystals, which became smaller as the temperature of liquid nitrogen decreased, but the temperature of −100 °C LNF was too low and might freeze and crack the samples, thus leading to a higher cooking loss. This result was consistent with Yang et al. (2022), LNF at −115 °C resulted in freeze-crack and reduced the quality of fish.

Thawing loss was an important indicator of the degree of muscle water loss during thawing and was associated with the texture, tissue state, and sensory evaluation of *C. gigas* (Lorentzen et al., 2020). Thawing loss was related to the size and distribution of ice crystals, the thawing speed, and the structural integrity of the muscle tissue (Ma, Mei, & Xie, 2021). As shown in Fig. 2C, the thawing loss in the −20 °C RF group was significantly higher than that in the LNF group ($P < 0.05$). As the temperature of liquid nitrogen decreased, the thawing loss also increased, with the −80 °C LNF group having the lowest thawing loss. In addition, the −80 °C LNF group significantly reduced thawing losses by 7.71% compared to the −20 °C RF group. The reduction in thawing loss was associated with the formation of small and homogeneous ice crystals. The samples treated with LNF formed small and homogeneous ice crystals, thus reducing the damage to muscle tissue cells during freezing. The samples treated with RF prolonged the freezing time, causing water to move outside the cells, forming large and irregular ice crystals on the outside, which could damage the structure of muscle tissue cells and lead to the formation of higher thawing loss (Xia et al., 2009). A similar result was reported by Sun et al. (2021), the mechanism of ultrasonic-assisted thawing (UT) reducing thawing loss was related to the formation of small ice crystals, which result in less damage to the muscle structure during freezing.

The results showed that LNF could maintain the WHC of *C. gigas* samples, among them, −40 °C LNF, −60 °C LNF, and −80 °C LNF groups could effectively improve the WHC of *C. gigas*. This was mainly because LNF could accelerate the freezing rate during the freezing process of food products, promote the formation of small ice crystals and reduce the damage to the muscle tissue structure of *C. gigas*. At the same time, LNF could maintain the stability of *C. gigas* myosin more effectively, thus maintaining the muscle structure (Li et al., 2019).

3.3. Effect of liquid nitrogen freezing at different temperatures on hardness of C. gigas

Hardness was an important indicator of *C. gigas* freshness and was related to the size of ice crystals, muscle water loss, and tissue integrity (Liu, Liang, Xia, Regenstein, & Zhou, 2013; Meral et al., 2019). The hardness of the body trunk and adductor muscles of *C. gigas* was shown in Fig. 2D and E. The hardness of the adductor muscles of *C. gigas* was greater than that of the body trunk muscles, with the fresh samples having the highest hardness, followed by −80 °C LNF, −60 °C LNF, −100 °C LNF, −40 °C LNF, −20 °C LNF and −20 °C RF. As could be seen in Fig. 2D, the fresh group was compared to the −60 °C LNF, and −80 °C LNF was not statistically significant ($P > 0.05$). Fig. 2E showed that there was no statistical significance ($P > 0.05$) between the fresh group and −60 °C LNF, −80 °C LNF, and −100 °C LNF. This result indicated that liquid nitrogen at a certain temperature could effectively maintain *C. gigas* muscle tissue structure and maintain the hardness of *C. gigas*. Furthermore, there was a link between hardness values and WHC, as water played an important role in shaping muscle structure, and this result for hardness was consistent with the WHC results. This present result was similar to that of Yang et al. (2022) on golden pompano

(*Trachinotus ovatus*), which found that LNF was effective in maintaining the hardness of *Trachinotus ovatus*, with the −95 °C LNF treated samples having better results. RF had the lowest hardness of all the frozen samples, mainly because the slow freezing rate produced larger ice crystals that disrupted the muscle fibre structure, resulting in a decrease in hardness of the oyster samples. The results showed that −60 °C LNF and −80 °C LNF-treated samples produced smaller ice crystals and reduced the disruption of cell structure. In contrast, ultra-low liquid nitrogen temperatures (−100 °C) froze and cracked the samples, reducing water holding capacity and leading to a reduction in oyster hardness.

3.4. Effect of liquid nitrogen freezing at different temperatures on light microscopy of C. gigas

Muscle microstructure greatly influenced meat product quality, especially WHC, and was very important to analysis of the physical properties of meat (Islam, Zhang & Liu, 2015; Jiang et al., 2019; Puolanne & Halonen, 2010). The micrographs of *C. gigas* samples frozen with different freezing methods were shown in Fig. 3. Unfrozen *C. gigas* was expectantly considered as the control for microstructure comparison with the frozen treatments. Fresh samples had smaller and denser pores. Compared to other samples, −20 °C RF samples had the largest pores, followed by −20 °C LNF samples, probably due to the slower freezing rate of the samples, resulting in cell shrinkage and the formation of larger extracellular ice crystals. These ice crystals could disrupt the cellular tissue structure and cause muscle fibres to the pool, hence the −20 °C RF and −20 °C LNF samples showed large intercellular gaps and incomplete muscle tissue. The LNF samples showed relatively intact muscle cell structure and significantly smaller gaps compared to the RF samples, indicating that rapid freezing resulted in the formation of small, regular ice crystals, reducing damage to the cellular structure. In particular, the cell structure of the −80 °C LNF samples was relatively tightly connected compared to the other LNF groups with relatively intact myofibrillar tissue, whereas the cell structure of the −100 °C LNF samples was disrupted, probably because the temperature was so low that it froze the samples, causing intracellular fluid to escape and larger gaps to form between cells. Similarly, Yang et al. (2022) also found that larger ice crystals would appear and break down tissue cells under slow freezing conditions. Under −95 °C LNF conditions, the rate of ice crystal formation was higher than the rate of water migration, so fine and uniform ice crystals were formed inside and outside the cell, which minimized the solute concentration effect and ice crystal damage to the inner and periplasmic membranes, and the muscle fibers were tightly connected and the extracellular fluid was smaller, maintaining better integrity. Therefore, the muscle structure of Chironomus was better maintained under −80 °C LNF conditions.

3.5. Effect of liquid nitrogen freezing at different temperatures on electronic nose (e-nose) of C. gigas

Electronic nose was a sensor set imitating the human olfactory system (Chen et al., 2022). The metal oxide sensors in an E-nose imitated the actions of a biological olfactory organism (Al-Dalali, Li, & Xu, 2021). Built-in gas sensors could respond to specific volatile classes with different values (Chen et al., 2022). Fig. 4A showed PCA analysis diagram, which was a projection method applied to reduce data dimensions and optimize the feature vectors by extracting the principal components (Yu et al., 2009). The first two principal components (PC1 and PC2, respectively), were extracted as the final feature vectors (Hu et al., 2021). The contribution of the first principal component (PC1) was 96.33% and the contribution of the second principal component (PC2) was 2.71%. There was an overlap between the −20 °C RF and −20 °C LNF groups, and between the Fresh and −40, −60, −80, and −100 °C LNF groups; however, the −20 °C RF and −20 °C LNF groups were in a different location from the Fresh and cryogenic liquid nitrogen groups. This result indicated that the −20 °C RF and −20 °C LNF groups had similar flavor profiles, and the −40, −60, −80, and −100 °C LNF groups had flavor profiles similar to those of the Fresh group. Then, the −20 °C RF and −20 °C LNF groups were distinguished from the Fresh group and cryogenic liquid nitrogen groups, indicating that they had different flavor profiles. This difference between flavor profiles might be due to the fact that the −20 °C RF and −20 °C LNF groups disrupted the cell structure during freezing, accelerating the formation of aldehydes, ketones, esters and other volatile compounds. In contrast, the −40, −60, −80, and −100 °C LNF groups effectively maintained the cell structure during freezing, which resulted in more effective maintenance of oyster flavor.

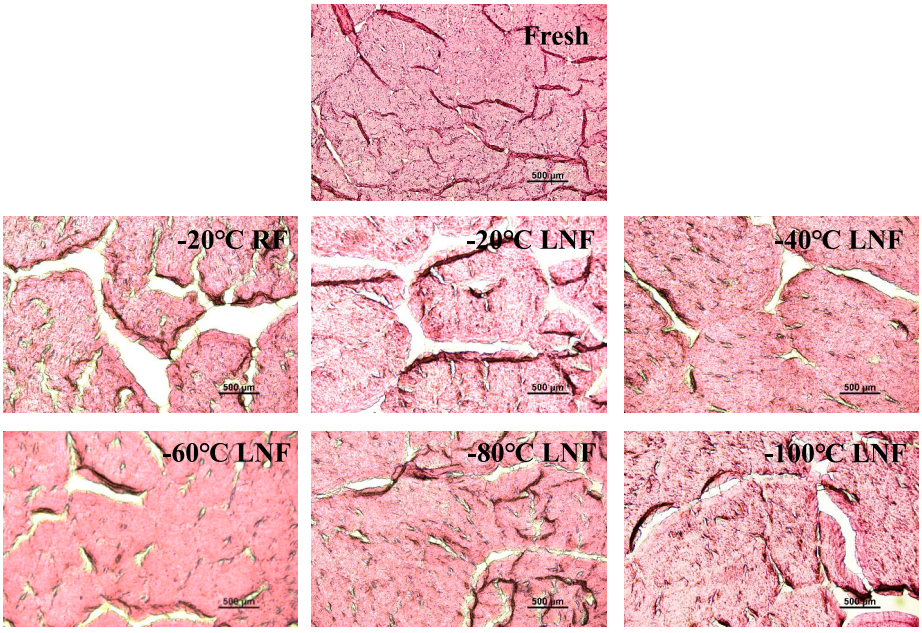

Fig. 3. Light microscope images of *C. gigas* with different freezing treatments.

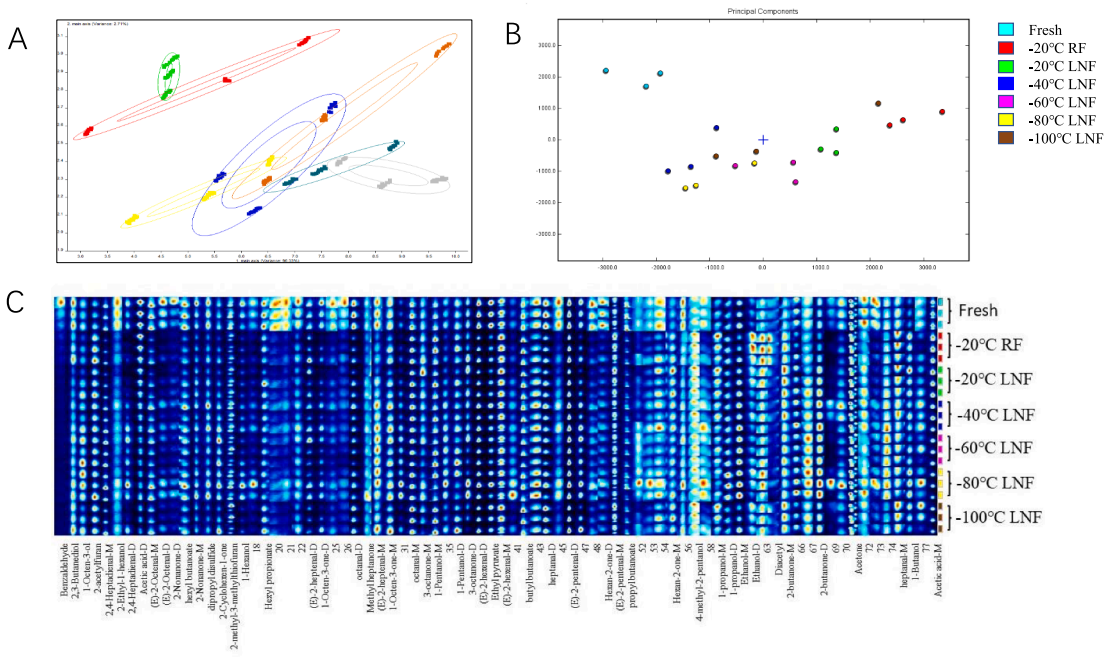

Fig. 4. Odor component analysis of *C. gigas* at different freezing treatments. (A) Principal component analysis (PCA) based on the electronic nose (E-nose) results; (B) PCA based on gas chromatography-ion mobility spectrometry (GC-IMS); (C) Fingerprint spectra of VOCs in *C. gigas* based on GC-IMS. Each row represents a VOC. Each column represents one sample.

3.6. Effect of liquid nitrogen freezing at different temperatures on volatile organic compounds (VOCs) of C. gigas

GC-IMS was used to analyze the VOC content in *C. gigas* under different freezing treatments. Fig. 4B showed that −20 °C RF and −20 °C LNF were farther away from the Fresh group in the score plot of PCA, indicating that the VOCs under this treatment had a significant effect on the Fresh group. As the liquid nitrogen temperature decreased, the −40 °C LNF, −60 °C LNF, −80 °C LNF, and −100 °C LNF groups were closer to the Fresh group, indicating that the VOCs in the low-temperature liquid nitrogen group were similar to those in the Fresh group. This result was consistent with the electronic nose results.

As shown in Fig. 4C, the fingerprint showed the distribution of volatile compounds. 51 VOCs were identified qualitatively, including 12 alcohols, 15 aldehydes, 5 esters, 11 ketones, 2 furans, 1 sulfide, and other compounds (Table 2) by searching the NIST database and IMS database (Feng, Ng, Mikš-Krajnik, & Yang, 2016), which was similar to (Feng et al., 2016). Notably, the same compound could detect small monomers and dimers and distinguish them from high-density monomer ions. Using the gallery plot plug-in of LAV, the signal peak intensities of each component without using the sample species were compared, and the results were visually displayed through fingerprint spectra. The formation of VOCs was associated with the degradation of lipids and proteins (Tian et al., 2020). Meanwhile, *C. gigas* treated by different freezing methods had different degradation pathways among the groups, resulting in different metabolites and different flavor compositions exhibited by each group (Li et al., 2021). Aldehydes and alcohols were important volatile odors in VOCs, with aldehydes having a relatively low threshold and a significant impact on the flavor of oysters (Wang et al., 2022). From the fingerprint plot, it was observed that the Fresh group was richer in VOCs and the frozen group had fewer VOCs. In the experiment, the concentrations of (E)-2-Octenal, 2-Nonanone, 1-Hexanol, 1-Octen-3-ol, 2-Ethyl-1-hexanol, 1-propranol, 2,4-Heptadienal and Hexan-2-one were found to be the highest in the Fresh group, while these flavors were also present in the −80 °C LNF group and less in the other groups. In addition, (E)-2-heptenal was more abundant in the −40, −60, and −80 °C LNF groups. In the experiments, samples frozen by −20 °C RF group formed large and irregular ice crystals that disrupted the muscle cell structure. The −80 °C LNF group could form smaller ice crystals, slowing down the degradation of proteins and lipids, which could effectively maintain the flavor substances in oysters.

3.7. Schematic illustration

In this study, a liquid nitrogen flash freezer was used to freeze the oysters, and the −20 °C RF was used as a control group to fully analyze the schematic diagram of the effects of different liquid nitrogen temperatures on the quality and flavor of *C. gigas*, as shown in Fig. S1 (He et al., 2022). The arrows in the graph represented the results of the liquid nitrogen group compared to the −20 °C RF group, with different colors representing different groups. As the liquid nitrogen temperature decreased, the freezing rate increased. −80 °C LNF could effectively improve the water holding capacity of oysters. Compared with RF, centrifugal loss was reduced by 9.61%, steaming loss by 3.78%, and thawing loss by 7.71%. Meanwhile, −80 °C LNF could effectively improve the hardness of oysters and better maintain the muscle tissue structure of oysters. Among them, the results of e-nose and GC-IMS were consistent, and the flavor composition of the fresh group and −80 °C LNF were similar. The results indicated that −80 °C LNF could effectively maintain the quality and flavor of oysters. The study also laid the foundation for the application of liquid nitrogen freezing technology.

4. Conclusion

This study compared the effects of refrigerator freezing and liquid nitrogen freezing at different temperatures on the quality and flavor changes in *C. gigas*. The results found that liquid nitrogen freezing could delay the quality deterioration of oysters to some extent. The total freezing time decreased with decreasing liquid nitrogen temperature; the freezing rate increased with decreasing liquid nitrogen temperature. −40, −60, and −80 °C LNF groups could effectively improve the WHC of *C. gigas*. −60 and −80 °C LNF groups reduced the damage to cell structure and slowed down the decrease of oyster hardness. −80 °C LNF group showed relatively intact muscle cell structure and fine gaps. E-

Table 2
GC-IMS integration parameters of VOCs in *C. gigas* at different liquid nitrogen temperatures.

Nos.	Compound	CAS#	Formula	MW	RI	Rt[*sec*]	Dt[RIPrel]
	Alcohols						
1	2,3-Butanediol	C513859	$C_4H_{10}O_2$	90.1	1523.7	1100.46	1.3685
2	1-Octen-3-ol	C3391864	$C_8H_{16}O$	128.2	1476.6	944.643	1.1541
3	2-Ethyl-1-hexanol	C104767	$C_8H_{18}O$	130.2	1486.6	975.609	1.4081
4	1-Hexanol	C111273	$C_6H_{14}O$	102.2	1368.4	664.934	1.3257
5	1-Pentanol-M	C71410	$C_5H_{12}O$	88.1	1268.7	485.277	1.2474
6	1-propanol-M	C71238	C_3H_8O	60.1	1036.9	249.101	1.1112
7	1-propanol-D	C71238	C_3H_8O	60.1	1039.6	250.857	1.2584
8	Ethanol-M	C64175	C_2H_6O	46.1	952.1	201.217	1.0439
9	Ethanol-D	C64175	C_2H_6O	46.1	930.8	191.332	1.1272
10	1-Butanol	C71363	$C_4H_{10}O$	74.1	1146.8	337.115	1.1766
11	1-Pentanol-D	C71410	$C_5H_{12}O$	88.1	1259.6	471.892	1.5036
12	4-methyl-2-pentanol	C108112	$C_6H_{14}O$	102.2	1164.7	355.106	1.272
	Aldehyde						
13	(E)-2-heptenal-D	C18829555	$C_7H_{12}O$	112.2	1333.2	594.071	1.6777
14	2,4-Heptadienal-M	C5910850	$C_7H_{10}O$	110.2	1469.5	923.077	1.1938
15	2,4-Heptadienal-D	C5910850	$C_7H_{10}O$	110.2	1460.4	895.982	1.6207
16	(E)-2-Octenal-M	C2548870	$C_8H_{14}O$	126.2	1422.4	792.198	1.33
17	(E)-2-Octenal-D	C2548870	$C_8H_{14}O$	126.2	1412.5	767.196	1.8224
18	octanal-D	C124130	$C_8H_{16}O$	128.2	1298.9	533.177	1.8246
19	(E)-2-heptenal-M	C18829555	$C_7H_{12}O$	112.2	1328.1	584.472	1.2567
20	octanal-M	C124130	$C_8H_{16}O$	128.2	1306.8	546.513	1.3987
21	(E)-2-hexenal-D	C6728263	$C_6H_{10}O$	98.1	1229.2	430.019	1.5149
22	(E)-2-hexenal-M	C6728263	$C_6H_{10}O$	98.1	1232.4	434.176	1.1823
23	heptanal-D	C111717	$C_7H_{14}O$	114.2	1193.6	386.576	1.7014
24	(E)-2-pentenal-D	C1576870	C_5H_8O	84.1	1140.4	330.971	1.3582
25	(E)-2-pentenal-M	C1576870	C_5H_8O	84.1	1140	330.683	1.1062
26	heptanal-M	C111717	$C_7H_{14}O$	114.2	1183.1	374.721	1.3377
27	Benzaldehyde	C100527	C_7H_6O	106.1	1538.6	1155.05	1.1485
	Ester						
28	hexyl butanoate	C2639636	$C_{10}H_{20}O_2$	172.3	1394.9	724.542	1.4762
29	Hexyl propionate	C2445763	$C_9H_{18}O_2$	158.2	1341.1	609.274	1.4239
30	Ethyl pyruvate	C617356	$C_5H_8O_3$	116.1	1249.2	457.041	1.1486
31	butyl butanoate	C109217	$C_8H_{16}O_2$	144.2	1205.5	400.503	1.3419
32	propyl butanoate	C105668	$C_7H_{14}O_2$	130.2	1104	298.687	1.263
	Ketones						
33	Methyl heptanone	C110930	$C_8H_{14}O$	126.2	1345.6	618.092	1.172
34	1-Octen-3-one-M	C4312996	$C_8H_{14}O$	126.2	1313.5	558.171	1.2667
35	1-Octen-3-one-D	C4312996	$C_8H_{14}O$	126.2	1308.8	550.006	1.6732
36	3-octanone-M	C106683	$C_8H_{16}O$	128.2	1275	494.902	1.3056
37	3-octanone-D	C106683	$C_8H_{16}O$	128.2	1258.5	470.238	1.7156
38	Hexan-2-one-D	C591786	$C_6H_{12}O$	100.2	1092.3	289.175	1.505
39	Hexan-2-one-M	C591786	$C_6H_{12}O$	100.2	1090.9	288.022	1.1875
40	2-butanone-M	C78933	C_4H_8O	72.1	892.3	175.239	1.0672
41	2-butanone-D	C78933	C_4H_8O	72.1	895.3	176.416	1.2405
42	Acetone	C67641	C_3H_6O	58.1	796.4	143.632	1.1266
43	2-Cyclohexen-1-one	C930687	C_6H_8O	96.1	1400	736.572	1.1112
44	Diacetyl	C431038	$C_4H_6O_2$	86.1	961	205.615	1.1627
	Furans						
45	2-acetylfuran	C1192627	$C_6H_6O_2$	110.1	1466.2	913.124	1.1126
46	2-methyl-3-methylthiofuran	C63012975	C_6H_8OS	128.2	1361.4	650.169	1.1036
	Sulfur compound						
47	dipropyl disulphide	C629196	$C_6H_{14}S_2$	150.3	1399.1	734.385	1.2617
	Other						
48	Acetic acid-D	C64197	$C_2H_4O_2$	60.1	1445.9	854.805	1.1596
49	2-nonanone-D	C821556	$C_9H_{18}O$	142.2	1384.7	701.027	1.8751
50	2-Nonanone-M	C821556	$C_9H_{18}O$	142.2	1386.4	704.855	1.4085
51	Acetic acid-M	C64197	$C_2H_4O_2$	60.1	1451.8	871.389	1.0488

MW, molecular mass; RI, retention index; Rt, retention time; Dt, drift time; D, means dimer; M, means monomer.

Compounds were identified by comparison with reference substances from the NIST and IMS library and presented in three replicates.

nose and GC-IMS results showed similar results, and the −80 °C LNF group could effectively maintain the flavor characteristics of oysters compared with other groups. In conclusion, the −80 °C LNF group could improve oyster quality and maintained flavor characteristics. The results of this study proved that −80 °C LNF could improve the quality of frozen oysters, which was of guiding significance and laid the foundation for the future application of liquid nitrogen freezing technology.

CRediT authorship contribution statement

Xiaoyu Teng: Conceptualization, Investigation, Data curation, Formal analysis, Writing – original draft. **Yu Liu:** Methodology. **Lipin Chen:** Investigation, Visualization, Writing – review & editing. **Changhu Xue:** Project administration, Supervision. **Zhaojie Li:** Conceptualization, Validation, Project administration.

Declaration of Competing Interest

The authors declare that they have no known competing financial interests or personal relationships that could have appeared to influence the work reported in this paper.

Data availability

Data will be made available on request.

Acknowledgments

This work was supported by National Key R&D Program of China (2019YFD0901802) and the earmarked fund for the Modern Agro-industry Technology Research System (CARS-49).

Appendix A. Supplementary data

Supplementary data to this article can be found online at https://doi.org/10.1016/j.foodchem.2023.136162.

References

Al-Dalali, S., Li, C., & Xu, B. (2021). Effect of frozen storage on the lipid oxidation, protein oxidation, and flavor profile of marinated raw beef meat. *Food Chemistry, 376*, Article 131881.

Botta, R., Asche, F., Borsum, J. S., & Camp, E. V. (2020). A review of global oyster aquaculture production and consumption. *Marine Policy, 117*, Article 103952.

Chen, L., Zhang, H., Shi, H., Xue, C., Wang, Q., Yu, F., … Li, Z. (2022). The flavor profile changes of Pacific oysters (*Crassostrea gigas*) in response to salinity during depuration. *Food Chemistry: X, 16*, Article 100485.

Dalvi-Isfahan, M., Hamdami, N., & Le-Bail, A. (2016). Effect of freezing under electrostatic field on the quality of lamb meat. *Innovative Food Science & Emerging Technologies, 37*, 68–73.

Espinoza Rodezno, L. A., Sundararajan, S., Solval, K. M., Chotiko, A., Li, J., Zhang, J., … Sathivel, S. (2013). Cryogenic and air blast freezing techniques and their effect on the quality of catfish fillets. *LWT - Food Science and Technology, 54*(2), 377–382.

Feng, X., Ng, V. K., Mikš-Krajnik, M., & Yang, H. (2016). Effects of fish gelatin and tea polyphenol coating on the spoilage and degradation of myofibril in fish fillet during cold storage. *Food and Bioprocess Technology, 10*(1), 89–102.

Gao, W., Hou, R., & Zeng, X.-A. (2019). Synergistic effects of ultrasound and soluble soybean polysaccharide on frozen surimi from grass carp. *Journal of Food Engineering, 240*, 1–8.

He, Y., Xie, Z., Xu, Y., Zhao, X., Zhao, L., & Yang, H. (2022). Preservative effect of slightly acid electrolysed water ice generated by the developed sanitising unit on shrimp (*Penaeus vannamei*). *Food Control, 136*, Article 108876.

Hong, H., Luo, Y., Zhou, Z., Bao, Y., Lu, H., & Shen, H. (2013). Effects of different freezing treatments on the biogenic amine and quality changes of bighead carp (*Aristichthys nobilis*) heads during ice storage. *Food Chemistry, 138*(2–3), 1476–1482.

Hu, M., Wang, S., Liu, Q., Cao, R., & Xue, Y. (2021). Flavor profile of dried shrimp at different processing stages. *Lwt, 146*, Article 111403.

Huang, X. H., Qi, L. B., Fu, B. S., Chen, Z. H., Zhang, Y. Y., Du, M., … Qin, L. (2019). Flavor formation in different production steps during the processing of cold-smoked Spanish mackerel. *Food Chemistry, 286*, 241–249.

Islam, M. N., Zhang, M., Liu, H., & Xinfeng, C. (2015). Effects of ultrasound on glass transition temperature of freeze-dried pear (*Pyrus pyrifolia*) using DMA thermal analysis. *Food and Bioproducts Processing, 94*, 229–238.

Jia, S., Li, Y., Zhuang, S., Sun, X., Zhang, L., Shi, J., … Luo, Y. (2019). Biochemical changes induced by dominant bacteria in chill-stored silver carp (*Hypophthalmichthys molitrix*) and GC-IMS identification of volatile organic compounds. *Food Microbiol, 84*, Article 103248.

Jiang, Q., Jia, R., Nakazawa, N., Hu, Y., Osako, K., & Okazaki, E. (2019). Changes in protein properties and tissue histology of tuna meat as affected by salting and subsequent freezing. *Food Chemistry, 271*, 550–560.

Li, D., Qin, N., Zhang, L., Li, Q., Prinyawiwatkul, W., & Luo, Y. (2019). Degradation of adenosine triphosphate, water loss and textural changes in frozen common carp (*Cyprinus carpio*) fillets during storage at different temperatures. *International Journal of Refrigeration, 98*, 294–301.

Li, D., Zhu, Z., & Sun, D.-W. (2018). Effects of freezing on cell structure of fresh cellular food materials: A review. *Trends in Food Science & Technology, 75*, 46–55.

Li, R., Guo, M., Liao, E., Wang, Q., Peng, L., Jin, W., & Wang, H. (2022). Effects of repeated freezing and thawing on myofibrillar protein and quality characteristics of marinated Enshi black pork. *Food Chemistry, 378*, Article 131994.

Li, S., Tian, Y., Jiang, P., Lin, Y., Liu, X., & Yang, H. (2021). Recent advances in the application of metabolomics for food safety control and food quality analyses. *Critical Reviews Food Science Nutrition, 61*(9), 1448–1469.

Liu, D., Liang, L., Xia, W., Regenstein, J. M., & Zhou, P. (2013). Biochemical and physical changes of grass carp (*Ctenopharyngodon idella*) fillets stored at -3 and 0 degrees C. *Food Chemistry, 140*(1–2), 105–114.

Lopkulkiaert, W., Prapatsornwattana, K., & Rungsardthong, V. (2009). Effects of sodium bicarbonate containing traces of citric acid in combination with sodium chloride on yield and some properties of white shrimp (*Penaeus vannamei*) frozen by shelf freezing, air-blast and cryogenic freezing. *LWT - Food Science and Technology, 42*(3), 768–776.

Lorentzen, G., Hustad, A., Lian, F., Grip, A. E., Schrødter, E., Medeiros, T., & Siikavuopio, S. I. (2020). Effect of freezing methods, frozen storage time, and thawing methods on the quality of mildly cooked snow crab (*Chionoecetes opilio*) clusters. *Lwt, 123*, Article 109103.

Ma, X., Mei, J., & Xie, J. (2021). Effects of multi-frequency ultrasound on the freezing rates, quality properties and structural characteristics of cultured large yellow croaker (*Larimichthys crocea*). *Ultrason Sonochem, 76*, Article 105657.

Meral, R., Alav, A., Karakas, C., Dertli, E., Yilmaz, M. T., & Ceylan, Z. (2019). Effect of electrospun nisin and curcumin loaded nanomats on the microbial quality, hardness and sensory characteristics of rainbow trout fillet. *Lwt, 113*, Article 108292.

Peng, D., Zhang, S., Zhang, H., Pang, D., Yang, Q., Jiang, R., … Zhu, Y. (2021). The oyster fishery in China: Trend, concerns and solutions. *Marine Policy, 129*.

Puolanne, E., & Halonen, M. (2010). Theoretical aspects of water-holding in meat. *Meat Science, 86*(1), 151–165.

Sun, Q., Chen, Q., Xia, X., Kong, B., & Diao, X. (2019). Effects of ultrasound-assisted freezing at different power levels on the structure and thermal stability of common carp (*Cyprinus carpio*) proteins. *Ultrason Sonochem, 54*, 311–320.

Sun, Q., Kong, B., Liu, S., Zheng, O., & Zhang, C. (2021). Ultrasound-assisted thawing accelerates the thawing of common carp (*Cyprinus carpio*) and improves its muscle quality. *Lwt, 141*, Article 111080.

Sun, Q., Sun, F., Xia, X., Xu, H., & Kong, B. (2019). The comparison of ultrasound-assisted immersion freezing, air freezing and immersion freezing on the muscle quality and physicochemical properties of common carp (*Cyprinus carpio*) during freezing storage. *Ultrason Sonochem, 51*, 281–291.

Teng, X., Cong, X., Chen, L., Wang, Q., Xue, C., & Li, Z. (2022). Effect of repeated freeze-thawing on the storage quality of pacific oyster (*Crassostrea gigas*). *Journal of Food Measurement and Characterization, 16*(6), 4641–4649.

Tian, X., Li, Z. J., Chao, Y. Z., Wu, Z. Q., Zhou, M. X., Xiao, S. T., … Zhe, J. (2020). Evaluation by electronic tongue and headspace-GC-IMS analyses of the flavor compounds in dry-cured pork with different salt content. *Food Research International, 137*, Article 109456.

Wang, Q., Sun, C., Chen, L., Shi, H., Xue, C., & Li, Z. (2022). Evaluation of microalgae diets on flavor characteristics of Pacific oysters (*Crassostrea gigas*) during fattening. *Food Chemistry, 391*, Article 133191.

Wu, Z., Ma, W., Xian, Z., Liu, Q., Hui, A., & Zhang, W. (2021). The impact of quick-freezing methods on the quality, moisture distribution and microstructure of prepared ground pork during storage duration. *Ultrason Sonochem, 78*, Article 105707.

Xia, X., Kong, B., Liu, Q., & Liu, J. (2009). Physicochemical change and protein oxidation in porcine longissimus dorsi as influenced by different freeze-thaw cycles. *Meat Science, 83*(2), 239–245.

Yang, F., Jing, D., Diao, Y., Yu, D., Gao, P., Xia, W., … Zhan, X. (2020). Effect of immersion freezing with edible solution on freezing efficiency and physical properties of obscure pufferfish (*Takifugu Obscurus*) fillets. *Lwt, 118*, Article 108762.

Yang, S., Hu, Y., Takaki, K., Yu, H., & Yuan, C. (2021). Effect of water ice-glazing on the quality of frozen swimming crab (*Portunus trituberculatus*) by liquid nitrogen spray freezing during frozen storage. *International Journal of Refrigeration, 131*, 1010–1015.

Yang, Z., Liu, S., Sun, Q., Zheng, O., Wei, S., Xia, Q., … Xu, J. (2022). Insight into muscle quality of golden pompano (*Trachinotus ovatus*) frozen with liquid nitrogen at different temperatures. *Food Chemistry, 374*, Article 131737.

Yu, H., Wang, J., Xiao, H., & Liu, M. (2009). Quality grade identification of green tea using the eigenvalues of PCA based on the E-nose signals. *Sensors and Actuators B: Chemical, 140*(2), 378–382.

Zhu, Z., Zhou, Q., & Sun, D.-W. (2019). Measuring and controlling ice crystallization in frozen foods: A review of recent developments. *Trends in Food Science & Technology, 90*, 13–25.